ORIGINAL RESEARCH

Check for updates

Antimony-Doped Tin Oxide Nanofibers as Catalyst Support Structures for the Methanol Oxidation Reaction in Direct Methanol Fuel Cells

Gaoyang Liu[1,2] • Arman Bonakdarpour[1] • Xindong Wang[2] • Xiaotao Bi[1] • David P. Wilkinson[1]

Abstract

One-dimensional (1-D) antimony-doped tin oxide nanofibers (ATO NF) were synthesized with the electrospinning method and were employed as Pt catalyst support materials for the methanol oxidation reaction (MOR). Scanning and transmission electron microscopy (SEM/TEM) indicate that the ATO NF exhibits a porous nanofiber structure and the diameters are in the range of 100 to 150 nm consisting of the stacked small ATO nanoparticles. Uniformly dispersed Pt nanoparticles were then deposited onto the ATO NF and the synthesized ATO nanoparticles (ATO NP) with a Pt loading of 20 wt%. Compared with the commercial Pt/C catalysts, both the ATO NF– and ATO NP–supported catalysts showed slightly lower electrochemical surface areas (ECSA) and catalytic activity towards the MOR. However, ATO NF, when used as Pt support, showed enhanced MOR stability. This enhancement is mainly attributed to the greater corrosion resistance and porous nanofiber nature of the ATO NF, which tend to inhibit the aggregation of anchored Pt nanoparticles and reduce the loss of ECSA during the accelerated life test. XPS results also indicate strong interactions between platinum and ATO particles, which in turn significantly enhance stability towards MOR.

Keywords Methanol oxidation reaction · Antimony-doped tin oxide · Nanofiber · Direct methanol fuel cells · Platinum catalysts

Introduction

Methanol is a promising energy carrier, and, as a liquid, it is easier than hydrogen and natural gas to store energy. Worldwide, 138 billion liters per year of methanol is produced from various energy sources [1]. Direct methanol fuel cells (DMFCs) provide an alternative pathway for methanol utilization, which have the potential to be practical sources of electrical power for applications in vehicles and stationary and portable electronic devices, owing to their advantages, such as high theoretical energy density, clean energy conversion, liquid fuel, and ease of use [2–4]. However, the commercialization of DMFC technology is still hindered by the high cost of noble metals and the poor durability of catalysts [5]. Thus, for successful commercialization of this technology, catalysts with improved activity and stability at lower precious metal loadings need to be developed [6].

Most active catalysts for the methanol oxidation reaction (MOR) on the anodic side of DMFCs, especially below 80 °C, are still those of Pt-based materials [7, 8]. In general, these catalysts consist of fine Pt nanoparticles supported on high surface area carbon materials such as Vulcan XC-72 [9], carbon nanotubes (CNTs) [10], and graphene [11]. The high activity of these supported catalysts is primarily due to the high dispersion and large surface area which lead to high utilization and low Pt loading. However, the carbon-based support materials can be oxidized to carbon dioxide at electrochemical potentials above 0.207 V versus NHE [12] and tend to suffer from corrosion degradation which is initiated in the electrooxidative environment of the anode and is likely accelerated in the presence of Pt nanoparticles [13, 14]. In addition, the stability of the electrocatalyst is also compromised because of the severe agglomeration or growth of Pt nanoparticles that occurs under fuel cell operation conditions [15]. In recent years, a number of metal oxides and ceramics such as SnO_2

✉ Xiaotao Bi
tony.bi@ubc.ca

✉ David P. Wilkinson
dwilkinson@chbe.ubc.ca

[1] Department of Chemical and Biological Engineering and the Clean Energy Research Center, University of British Columbia, 2360 East Mall, Vancouver, BC V6T 1Z3, Canada

[2] Department of Physical Chemistry, University of Science and Technology Beijing, 30 College Road, Beijing 100083, China

 Springer

[16], CeO$_2$ [17], NbO$_2$ [18], and WO$_3$ [19] were developed as electrocatalyst support materials due to their outstanding oxidation and excellent acid corrosion resistance [20]. However, because of the low electrical conductivity of these materials, a high mass ratio of Pt has to be used with those support materials. Another strategy has been the development of more conductive supports like Ti$_n$O$_{2n-1}$ (4 < n < 9) [21], NbC [22], TiC [23], and antimony-doped tin oxide (ATO) [24]. Among these, ATO has been proposed as a potential support material due to its excellent stability and high electrical conductivity [25, 26]. Moreover, it has been reported that an interactive support-catalyst effect could be operative between the ATO support and the Pt catalyst, which goes beyond the expected outstanding corrosion resistance and high electrical conductivity of ATO. Compared with the interaction between carbon support and Pt catalyst, on one hand, the ATO support has been reported to exhibit bi-functional effects by showing remarkable promotion in reducing CO poisoning thus enhancing the overall MOR rates [27]. On the other hand, The ATO could have a stabilizing effect on the Pt nanoparticles [28]. These properties of ATO could inhibit the detached Pt nanoparticles from forming agglomerates and electrochemical dissolution of Pt nanoparticles, which would increase the activity and stability of the Pt catalysts.

The low surface area of ATO materials compared with those of carbon-based materials has limited the performance of ATO-supported catalysts. To increase the surface area, ATO-modified carbon materials have been developed [29]. ATO carbon composite support materials have shown two conflicting impacts: (1) enhanced stability of the catalyst primarily due to their bi-functional effects and greater corrosion resistance [30] and (2) a decrease of the catalytic activity of Pt catalysts due to lower surface area and charge transfer capacity compared with pure carbon-based support materials [31]. Other advantages have been revealed from the ATO modified one-dimensional (1-D) nanostructured carbon nanotubes [32]. Compared with the carbon-supported Pt nanoparticles (Pt-NPs) one-dimensional (1-D) nanostructure materials provide the advantage of better charge transport properties and can effectively inhibit the aggregation of the anchored small Pt-NPs, and thus promote their catalytic activity over longer periods of time. Moreover, one-dimensional (1-D) nanostructure materials are thought to avoid full coverage with ionomer during the catalyst layer formation stage, thus improving the charge transfer rate in the catalyst layer [33].

In our previous work, one-dimensional (1-D) nanostructured ATO porous nanofibers have been developed and employed as a support for oxygen evolution (OER) catalysts. Even under the harsh operating environment of the anode, the ATO nanofiber supports result in a significantly improved stability [34]. In the present work, in order to completely avoid the use of carbon, we further employed the optimized ATO porous nanofiber as support of Pt catalysts. To elucidate the effect of the nanofiber structure and the ATO component on the catalytic activity and stability of the supported Pt, the ATO nanoparticles prepared by chemical co-precipitation and the commercial carbon nanoparticles were also used as support of Pt catalysts for comparison. All the support and the supported Pt catalysts were carefully characterized via various physical and electrochemical methods.

Experimental Methods

Chemicals Used for the Synthesis

All the chemicals used in the present work were analytically pure, unless otherwise specified, and used as received without further purification. Nafion® solution (5 wt%) was supplied by Dupont. Hexachloroplatinic acid (H$_2$PtCl$_6$), PTFE emulsion (6 wt%), and 20 wt% Pt/C were received from the Beijing Nonferrous Metal Research Institute, Shanghai Organic Fluorine Material Research Institute, and Johnson Matthey, respectively. Other chemicals were from Sinopharm Chemical Reagent Co. Ltd.

Synthesis of Catalyst Supports

The antimony-doped tin oxide nanofibers were synthesized by an optimized electrospinning method (homemade setup) as reported in the reported literatures [32, 35]. In the present work, in order to synthesize the antimony-doped tin oxide nanofibers with smaller diameters, we further adjusted several key parameters of the precursor solution for the electrospinning process. The antimony-doped tin oxide precursor solution in this study was prepared by dissolving 2 g the polyvinylpyrrolidone (PVP, Mw ≈ 1,300,000) in 40 mL methanol and 0.1 g of SnCl$_2$·2H$_2$O with 0.018 g of SbCl$_3$· 2H$_2$O in 40 mL methanol while stirring, and then, the solutions were mixed together. DI water was then added to the resulting precursor solution to achieve a water to methanol volume ratio of 1:3 before being loaded into a syringe for the electrospinning process. The as-spun precursor nanofibers were then calcined at 600 °C for 6 h in air under a heating rate of 0.5 °C min^{-1}, and the obtained antimony-doped tin oxide nanofibers are referred to as ATO NF. Antimony-doped tin oxide nanoparticles were also prepared via a co-precipitation method for comparison and are referred to as ATO NP. It should be pointed out that the content of Sb dopant for both the ATO NF and ATO NP is 5 mol% according to our earlier work [36].

Preparation of Supported Pt Catalysts

The ATO NF– and ATO NP–supported Pt catalysts were prepared by a modified polyol method [37]. Briefly,

hexachloroplatinic acid (1.93 mM) was dissolved in ethylene glycol. The pH value of the precursor solution was then adjusted to above 10 through a dropwise addition of 1.0 M NaOH dissolved in ethylene glycol under magnetic stirring. The precursor solution was refluxed at 160 °C for 3 h and then with the support materials being added. The pH value was slowly decreased to 2 by the dropwise addition of 0.1 M HCl. The mixture was kept at 90 °C for 3 h, and the entire preparation process was conducted under a flowing nitrogen atmosphere. The supported Pt catalysts were obtained after being cooled to room temperature, centrifugal separated and washed with distilled water, and then dried. The Pt loading for both the ATO NF– and ATO NP–supported catalysts was confirmed with XRF (X-ray fluorescence) analysis, and the mean Pt loadings in Pt/ATO NF and Pt/ATO NP samples were found to be ∼ 22 and ∼ 19 wt%, respectively. These results are very close to our nominal Pt loadings (20 wt%) in the catalysts.

Physiochemical Characterization

Structural analysis of the catalyst was performed by using an X-ray diffractometer (XRD) (MXP21 VAHF) equipped with a Cu-Kα radiation ($\lambda = 1.54056$ Å).

The morphology and particle size distribution of the prepared support materials were determined using scanning electron microscopy (SEM) (LEO-1530 Gemini FESEM, ZEISS) and transmission electron microscopy (TEM) (FEI Tecnai G2 F20 microscope) operated at an accelerating voltage of 300 kV.

The surface chemical composition of the catalyst was measured by XPS, which was performed using a Kratos Analytical XSAM-800 spectrometer equipped with an Al Kα monochromatic source at a power of 350 W. The C 1s photoelectron peak at 284.6 eV was used as the reference.

Electrochemical Characterization

For electrochemical evaluation, 5 mg catalyst powder was dispersed in 1 mL isopropyl alcohol (Analytically Pure, Beijing Chemical Factory), into which 50 μL Nafion® solution (5 wt%, Dupont) was added. The mixture was then homogenized for 1 h in an ice ultrasonic bath to form an ink. A 8.4-μL aliquot of the dispersed catalyst ink was pipetted on a graphite carbon substrate (UHP, Topfly Material Co., Ltd.) with a geometric area of 0.5 cm^2 and was dried at 75 °C in a vacuum oven. This coated graphite was used as a working electrode for the electrochemical measurement.

The electrochemical properties of the catalyst were characterized using a VMP2 potentiostat (Princeton Applied Research), a Pt coil (CHI120, ChenHua) as the counter electrode, and a saturated calomel electrode (SCE) (Model 217, LeiCi company) as the reference electrode at 25 °C. The SCE reference electrode was calibrated in 0.5 M H$_2$SO$_4$ solution saturated with H$_2$; a clean Pt wire was employed as the working electrode. All potentials collected to the SCE reference electrode are converted to potential with respect to the reversible hydrogen electrode with the following formula:

$$U_{RHE} = U_{SCE} + 0.059 \times pH + 0.24$$

The working electrodes were initially cleaned electrochemically by sweeping the potential between 0 and 1.40 V at 100 mV s^{-1} until steady-state CVs were obtained using a N$_2$-saturated 0.5 M H$_2$SO$_4$ electrolyte. CVs were then recorded in the potential range of 0.04 to 1.20 V at a slower scan rate of 50 mV s^{-1} for 20 cycles. A stable cycle (20th cycle) of the CVs was used for calculating the electrochemical surface area (ECSA) of Pt. For the MOR measurements, CVs were conducted in the potential range of 0.04 to 1.10 V at a scan rate of 20 mV s^{-1} in an electrolyte of 0.5 M H$_2$SO$_4$ and 1 M CH$_3$OH.

An accelerated life test was carried out by potential cycling in the potential range of 0.04 to 1.1 V at a scan rate of 50 mV s^{-1}. After the electrooxidation cycling of methanol for 4000 cycles, CVs were recorded in the potential range of 0.04 to 1.2 V in N$_2$-saturated 0.5 M H$_2$SO$_4$ and the corresponding ECSA values were then obtained.

Results and Discussions

XRD patterns of ATO NF, ATO NP, and the corresponding supported catalysts are shown in Fig. 1. Multi characteristic diffraction peaks for both the ATO NF and ATO NP could be observed and were matched well with the single-phase tetragonal rutile–structured SnO$_2$ (JCPDS 21-1250). It indicated that both the ATO NF and ATO NP possessed the polycrystalline structure. Furthermore, there are no diffraction peaks of antimony oxide and it indicated that substitutional doping has taken place. The successfully doped Sb in the SnO$_2$ lattice was expected to improve the electrical conductivity of ATO based on our previous study, which will not be further discussed in the present work. When the ATO NF and ATO NP were employed to support the Pt catalyst, it could be seen that the characteristic pattern of Pt diffraction in both the ATO NF and ATO NP supported Pt catalysts. The (111) Bragg peak of Pt (∼ 39.6°) is clearly visible, and other Bragg peaks of Pt at scattering angles of 46.3°, 68.7°, and 81.2° can be observed and are indexed to (200), (220), and (311) planes. The crystallite sizes of Pt nanoparticles loaded on different supports were further calculated with the Scherrer's equation. Small Pt of 1.9 nm and 3.6 nm were obtained for the Pt/ATO NF and Pt/ATO NP catalysts, respectively.
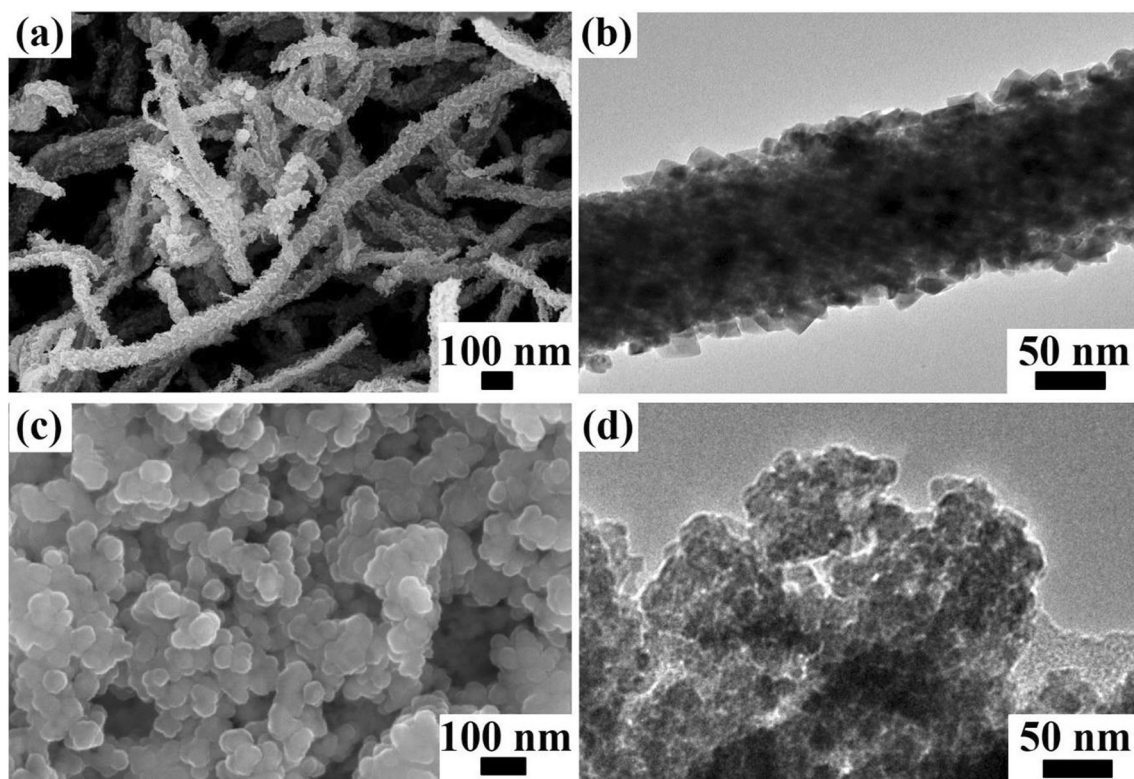
Figure 2 shows the SEM and TEM images of ATO NF and ATO NP. In order to decrease the diameters of the ATO NF, lower PVP concentrations in the precursor

Fig. 1 XRD patterns of the ATO NF and ATO NP, and the corresponding supported catalysts
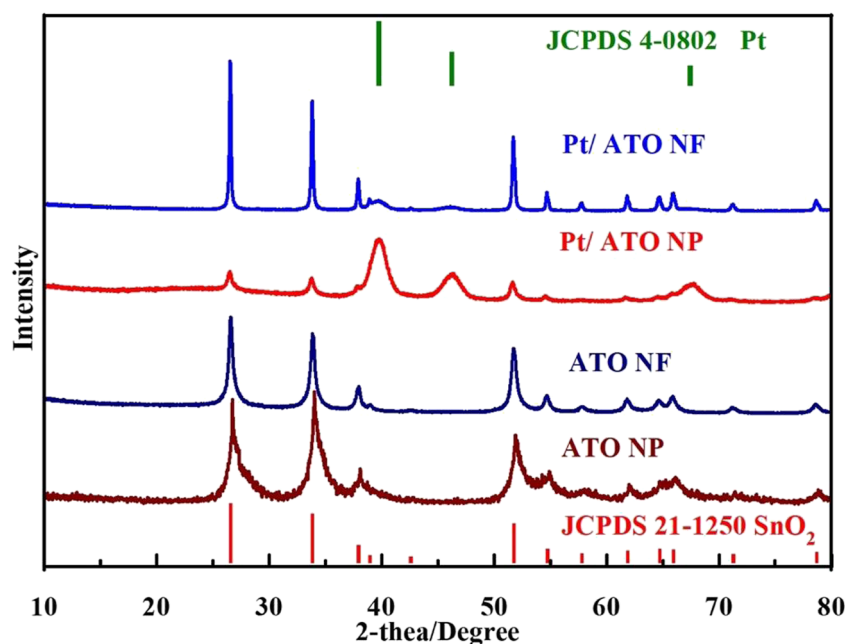
solution were used during the ATO NF preparation via the electrospinning method. It could be seen that the as-prepared ATO NF maintains the nanofiber structures with lengths of up to a few micrometers (Fig. 2a). It is also clear that the nanofibers have a very rough surface with surface protrusions, which increases the surface area of the support with fine ATO nanoparticles. The magnified

TEM (Fig. 2b) further confirms the porous nanofiber structure of the ATO NF with a diameter in the range of 100–150 nm, and the ATO NF primarily consists of small stacked ATO nanoparticles within a diameter range around 20 nm (Fig. 2b). For ATO NP, as shown in Fig. 2c, the prepared ATO NP has an independently distributed nanosphere structure within a narrow diameter range of

Fig. 2 SEM images of **a** ATO NF and **c** ATO NP, and TEM images of **b** ATO NF and **d** ATO NP

30–40 nm based on the SEM image and this is further confirmed by the TEM image (Fig. 2d).

Figure 3 shows TEM and HRTEM images of the synthesized Pt catalysts using ATO NF and ATO NP as support. TEM images (Fig. 3a, c) of the as-prepared catalysts show that the small Pt particles are uniformly distributed on both ATO NF and ATO NP supports, and the original structure of the support remains unchanged. Based on the measured lattice spacing of the crystal planes in the HRTEM images of Pt/ATO NF and Pt/ATO NP (Fig. 3b, d), both the (111) plane of Pt and the (110) plane of SnO_2 could be clearly identified in the HRTEM image of Pt/ATO NF and Pt/ATO NP; this observation is consistent with the XRD data (Fig. 1). These images further confirmed that Pt nanoparticles have been successfully deposited on ATO in both catalysts.

In order to investigate the interactive supported effect between the Pt and the support, the binding energy region of Pt 4f core electrons for Pt/ATO NF, Pt/ATO NP, and Pt/C were investigated by XPS (Fig. 4). The Pt $4f_{7/2}$ and Pt $4f_{5/2}$ peaks could be observed for all the prepared catalysts. For both the Pt/ATO NF and Pt/ATO NP, the Pt $4f_{7/2}$ and Pt $4f_{5/2}$ peaks occur at binding energies (BEs) of around 71.5 and 74.7 eV, respectively. However, for Pt/C, the Pt $4f_{7/2}$ and Pt $4f_{5/2}$ peaks appear at 71.1 eV and 74.2 eV, respectively. There is a shift to higher binding energy of the Pt $4f_{7/2}$ and Pt $4f_{5/2}$ doublet peaks for both the Pt/ATO NF and Pt/ATO NP, compared with the Pt/C. This change indicates that the electronic structure of Pt can be modified by ATO [38]. The supported Pt can donate electrons to the support, hence reducing the shielding effect of the outer electrons. This electron donation process is then manifested by the increase in the BE of Pt's core electrons in the 4f orbital. The electronic interaction between Pt and support can thus play an important role towards the MOR catalytic activity, as discussed in the later sections.

Figure 5 shows the CVs of Pt/C, Pt/ATO NF, and Pt/ATO NP in N_2-saturated 0.5 M H_2SO_4 electrolyte. The CVs of these three Pt catalysts exhibit all the characteristic features of clean polycrystalline Pt. The reversible hydrogen adsorption/desorption peaks are clearly identified in the potential region of 0.04 to 0.34 V and are used to extract the electrochemical surface area of the catalysts. The H^+ adsorption charge density is determined by integrating the H^+

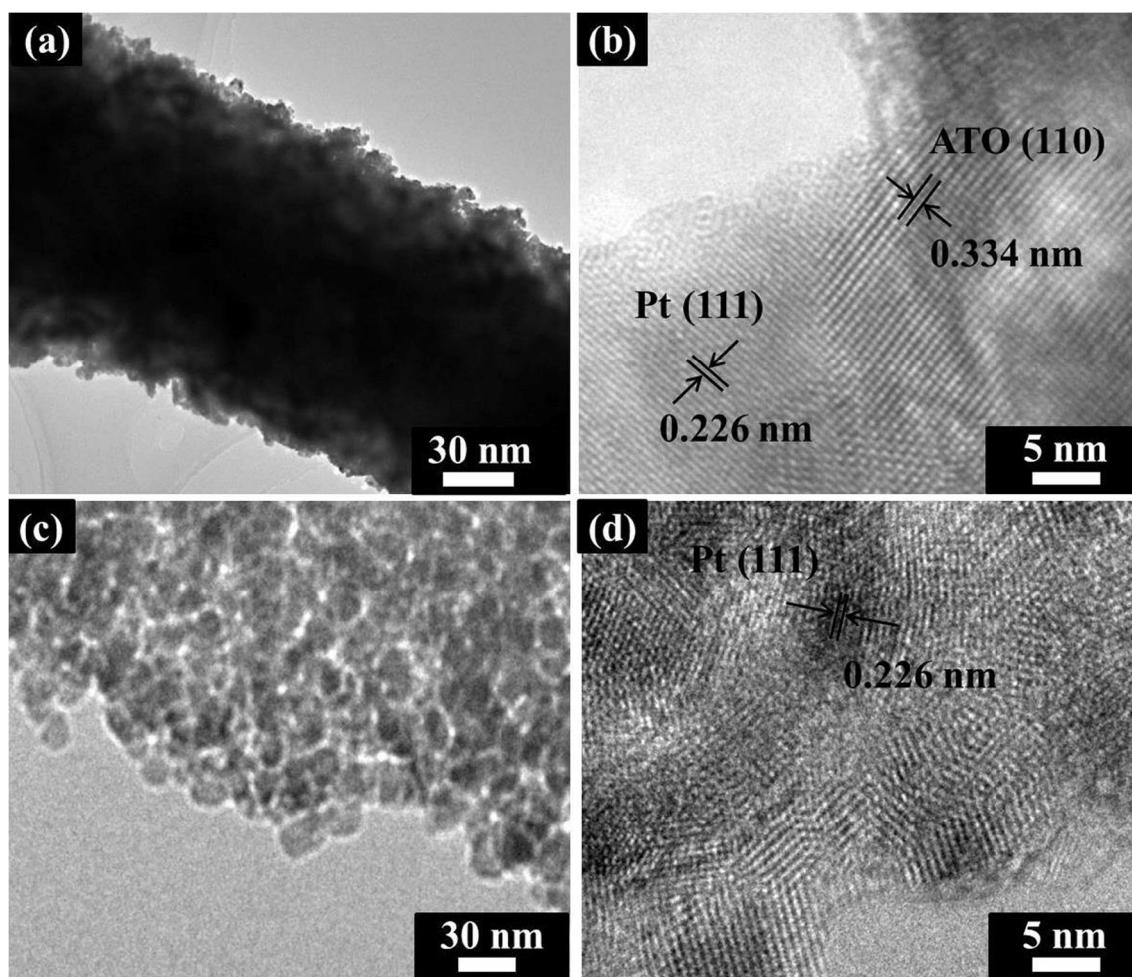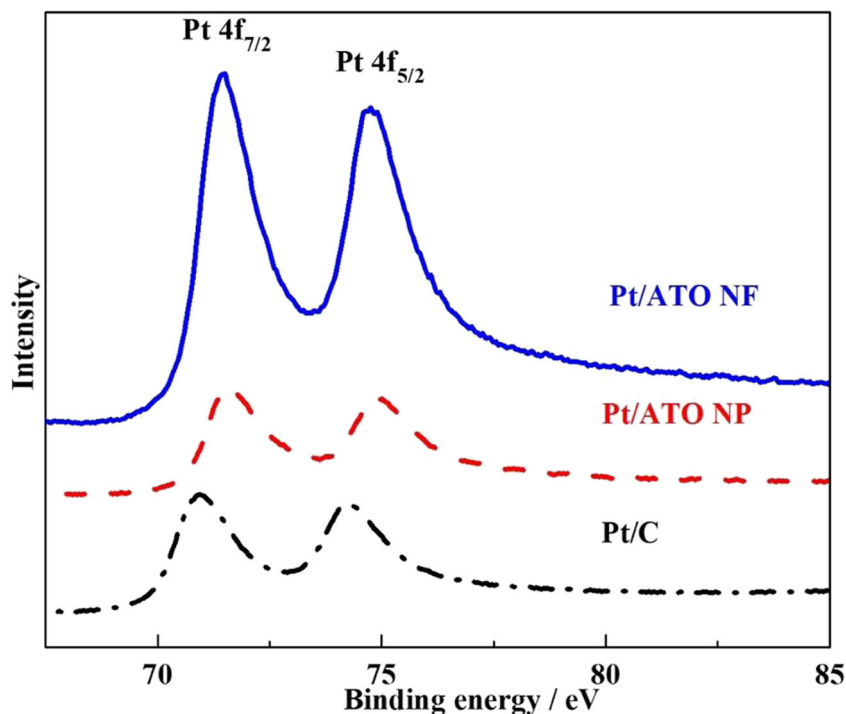**Fig. 3** TEM and the corresponding HRTEM images of Pt/ATO NF (**a**, **b**) and Pt/ATO NP (**c**, **d**)

Fig. 4 XPS spectra of Pt 4f in prepared Pt/ATO NF, Pt/ATO NP, and Pt/C


desorption peak area after correcting for the double-layer charging current. The Pt/ATO NP catalyst exhibited the smallest ECSA value (~ 26 m^2 g^{-1}) due to a gradual increase in the Pt particle size on the ATO NP support according to the XRD observation. A higher ECSA value (~ 33 m^2 g^{-1}) was obtained for Pt/ATO NF, which is most likely due to a better dispersion of Pt nanoparticles on the surface of the ATO NF, and a relatively lower charge transfer resistance of the 1-D nanostructured ATO NF. The ECSA of the commercial Pt/C was found to be much higher (~ 55 m^2 g^{-1}).

Figure 6 presents the mass normalized CVs of the prepared Pt electrocatalysts in 0.5 M H_2SO_4 + 1 M CH_3OH solution. Both the methanol oxidation peak (I_f, 0.8~0.9 V) in the positive scan and the oxidation peak associated with the oxidation of the intermediate carbonaceous species (e.g., CO_{ads}) (I_b, 0.7~0.8 V) in the negative scan were observed for all the catalysts. The current densities of the methanol oxidation peaks (I_f) were found to decrease in the order of Pt/C > Pt/ATO NF > Pt/ATO NP, indicated a decreasing mass activity of the

Fig. 5 CVs of Pt/C, Pt/ATO NP, and Pt/ATO NF catalysts in N_2-saturated 0.5 M H_2SO_4 solution at a scan rate of 50 mV s^{-1}
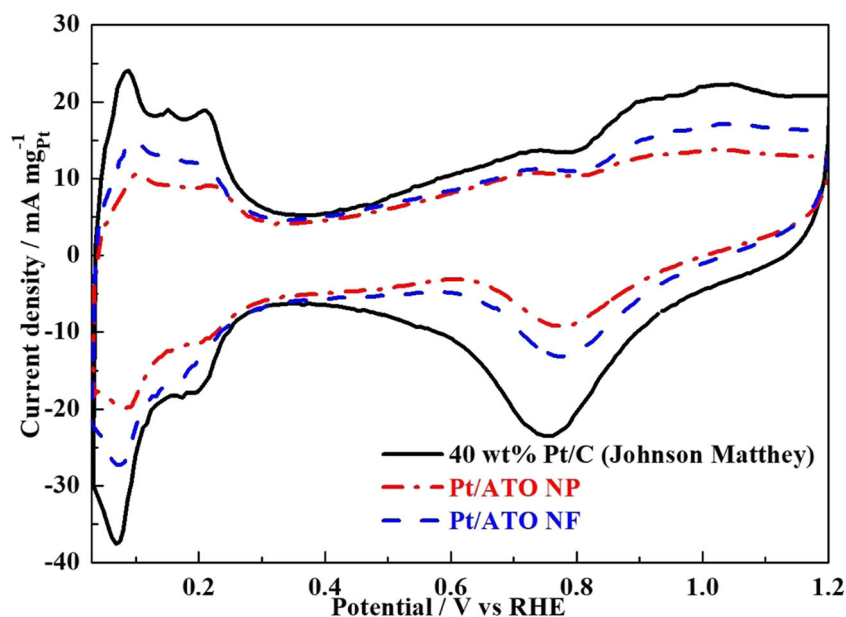
Fig. 6 Mass normalized CVs of Pt/C, Pt/ATO NP, and Pt/ATO NF catalysts in 0.5 M H_2SO_4 + 1 M CH_3OH solution at a scan rate of 20 mV s^{-1}
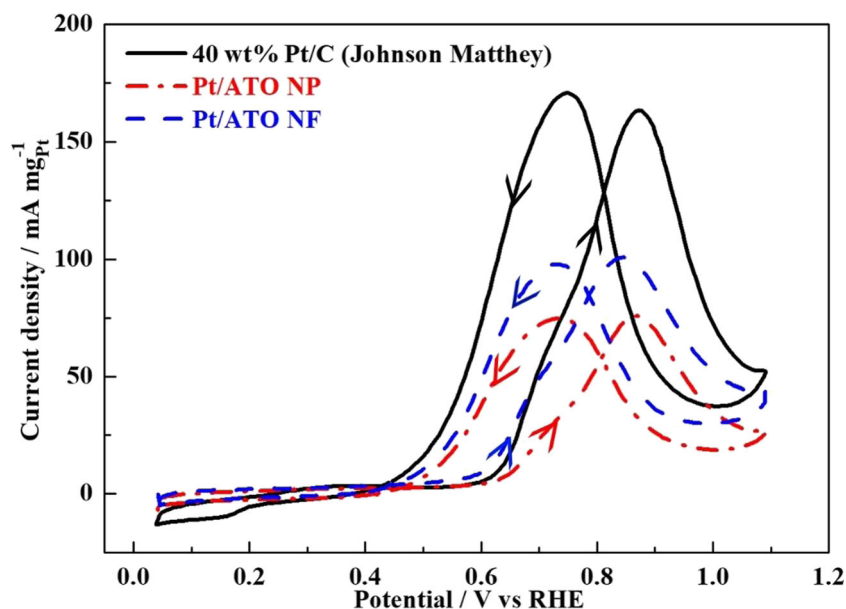
prepared Pt electrocatalysts towards the methanol oxidation reaction [34]. The current density of the methanol oxidation peak in the forward scan was used for calculating mass activity (Table 1). As shown in Table 1, the highest mass activity of the commercial Pt/C could be a result of the better distribution of the Pt nanoparticles on the carbon and/or the fine Pt nano-particle size, and it is consistent with the highest ECSA of the commercial Pt/C catalysts. In order to eliminate the geometric effect (related to the ECSA) of the support, the intrinsic activity of Pt on different supports was further analyzed via normalizing the measured current by the ECSA. Thus, obtained intrinsic activity of the prepared Pt catalysts slightly decreases in the order of Pt/ATO NF > Pt/ATO NP > Pt/C (Table 1). The increased intrinsic activity of Pt/ATO NF is probably caused by the better charge transport provided by the porous nanofiber structure, and also, ATO can improve the intrinsic activity of Pt towards MOR as reported by Xu et al. [34].

As previously reported by Arentzet et al. [39] and Santoset al. [16], H_2O can be easily dissociated on the surface of SnO_2 at a lower potential and lead to an OH_{ads}-rich surface on SnO_2, which will enhance the CO_{ads} oxidation on Pt, resulting in a higher I_f/I_b value. The ratio of the forward peak (I_f) to backward (I_b) peak current (I_f/I_b) was found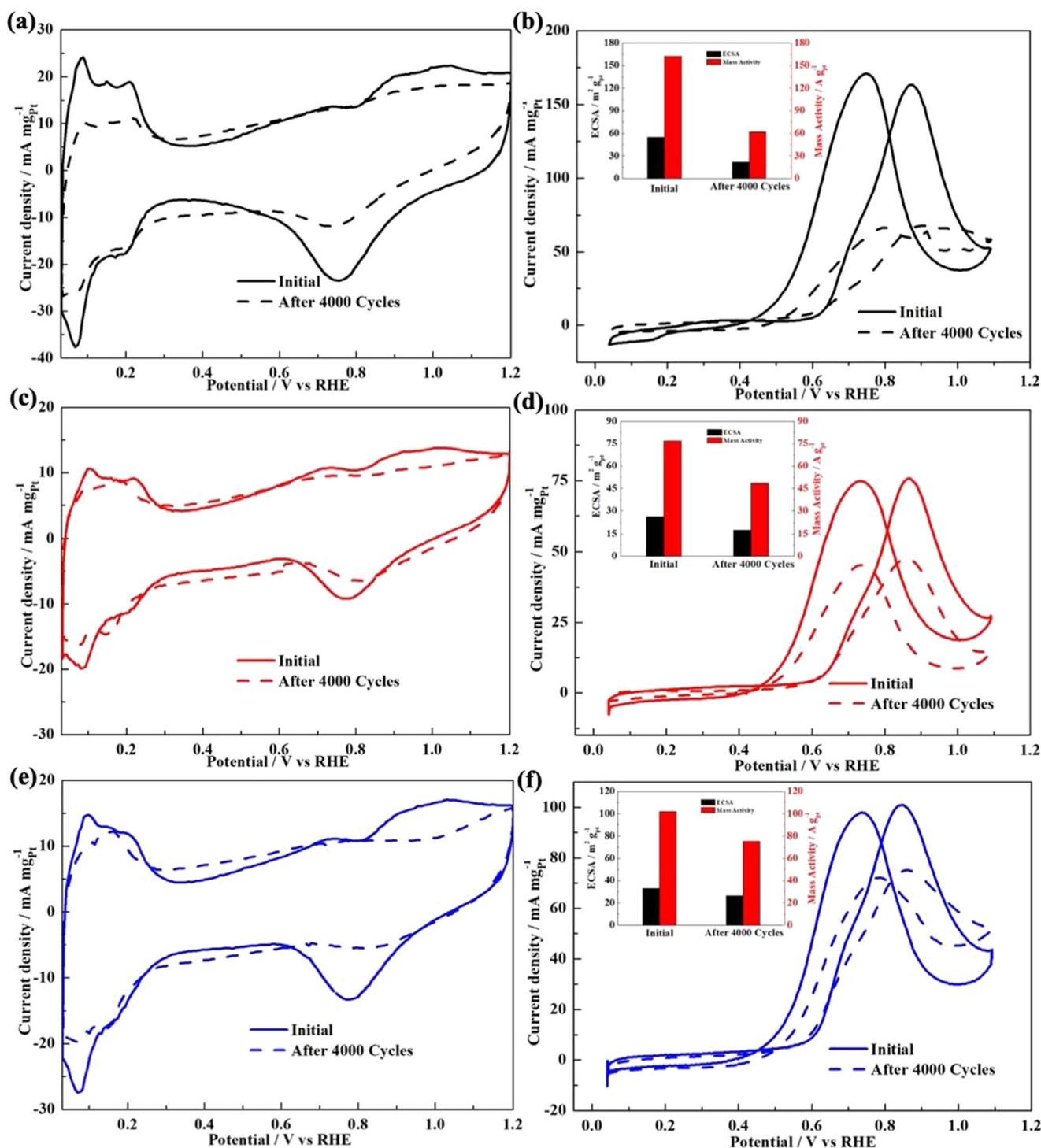 to decrease in the following order: Pt/ATO NF > Pt/ATO NP > Pt/C (Table 1). The I_f/I_b has been proposed to be a measure of the catalyst tolerance to intermediate carbonaceous species, and also, it is related to the catalytic activity [40]. The higher CO tolerance of the ATO-supported catalysts can be expected to promote stability towards the MOR.

The stability of anode catalysts still remains a key challenge for the present DMFC technology. The electrochemical stability of each catalyst was evaluated by performing repeated electrooxidation CVs of methanol, up to 4000 cycles. After the methanol electrooxidation measurements, CVs of the corresponding electrode were also recorded to obtain the corresponding ECSA in the potential range between 0.04 and 1.20 V in N_2-saturated 0.5 M H_2SO_4. The results of the initial and 4000th cycles are shown in Fig. 7. The insets in Fig. 7 show the corresponding ECSA and mass activity histograms of the catalysts.

As shown in Fig. 7, both the ECSA and the mass activity of Pt/ATO NF, Pt/ATO NP, and Pt/C at the 4000th cycle have decreased compared with the first cycle. The most severe decrease of the ECSA and the mass activity occurred for the Pt/C catalyst, with the losses of the ECSA and the mass activity reaching about 60% and 62%, respectively. For Pt/ATO NP catalyst, losses of the ECSA and the mass activity were 32% and 37%, respectively, and for the Pt/ATO NF catalysts, these values were 20% and 26%, respectively. The stability of

Table 1 Comparison of ECSA and MOR activity for different supported catalysts

	ECSA (m^2 g^{-1})	Mass activity (A g$_{Pt}^{-1}$)	Intrinsic activity (A m^{-2})	(I_f/I_b)
Pt/C	55	162	2.95	0.958
Pt/ATO NP	26	77	2.96	1.013
Pt/ATO NF	33	102	3.11	1.034

Fig. 7 CV curves for **a** Pt/C, **c** Pt/ATO NP, and **e** Pt/ATO NF before and after the MOR cycling for 4000 cycles at 50 mV s^{-1} in N$_2$-saturated 0.5 M H$_2$SO$_4$. Mass-normalized CV curves for **b** Pt/C, **d** Pt/ATO NP, and **f** Pt/ ATO NF before and after the MOR cycling for 4000 cycles at 20 mV s^{-1} in 0.5 M H$_2$SO$_4$ + 1 M CH$_3$OH solution. The inserts are the corresponding ECSA histograms

catalysts was found to decrease in the order of Pt/ATO NF > Pt/ATO NP > Pt/C. These results indicate that the substitution of carbon by ATO can greatly improve the overall stability of the supported Pt catalyst. Possible reasons for improved stability of these catalysts could be as follows.

- Repeated CVs for electrooxidation of methanol can lead to dissolution and loss of Pt or dissolution and precipitation to form larger particle size Pt.
- Oxidation of the carbon support is a well-known phenomenon which leads to platinum sintering. In addition, OH$_{ads}$

on the catalyst surface can also oxidize the carbon support, forming gaseous carbon dioxide. The overall results are the detachment and agglomeration of Pt nanoparticles, leading to a decrease in ECSA of the catalyst.

- A stronger interaction between the ATO support and Pt atoms or clusters could better anchor the Pt nanoparticles to the surface of the antimony tin oxide, thereby inhibiting potential Pt dissolution and migration, leading to better stability of the Pt catalyst.

Conclusions

Catalyst support structures consisting of porous nanofibers from antimony-doped tin oxide (ATO) were prepared via a simple and effective electrospinning method. Compared with the conventional Pt/C, the ATO NP–supported Pt catalysts exhibited improved stability for methanol oxidation reaction. The losses of the ECSA and the mass activity were 32% and 37%, respectively, which were much lower than those of Pt/C (60% and 62%). It could be concluded that the outstanding corrosion resistance of ATO as well as the promoted CO tolerance of the supported catalyst inhibited Pt migration and suppressed the growth of Pt particles. Moreover, due to the improved charge transfer capacity of the porous nanofiber ATO NF support, Pt/ATO NF catalyst reached lower loss of the ECSA and the mass activity (20% and 26%).

References

1. A. Marc, The changing face of the global methanol industry. IHS Chem. Bull. **3**, 10–11 (2016)
2. K.B. Prater, Solid polymer fuel cells for transport and stationary applications. J. Power Sources **61**(1–2), 105–109 (1996)
3. S.M.M. Ehteshami, S.H. Chan, A review of electrocatalysts with enhanced CO tolerance and stability for polymer electrolyte membrane fuel cells. Electrochim. Acta **93**(30), 334–345 (2013)
4. M. Chen, M. Wang, Z.Y. Yang, X.N. Ding, X.D. Wang, Long-term degradation behaviors research on a direct methanol fuel cell with more than 3000h lifetime. Electrochim. Acta **282**(20), 702–710 (2018)
5. M. Cao, D. Wu, R. Cao, Recent advances in the stabilization of platinum electrocatalysts for fuel-cell reactions. ChemCatChem **6**(1), 26–45 (2014)
6. Y. Feng, J.H. Yang, H. Liu, J. Yang, Selective electrocatalysts toward a prototype of the membraneless direct methanol fuel cell. Sci. Rep. **4**(3813), 1–7 (2014)
7. K. Piyush, D. Kingshuk, D. Suparna, P.K. Patit, An overview of unsolved deficiencies of direct methanol fuel cell technology: factors and parameters affecting its widespread use. Int. J. Energy Res. **38**(11), 1367–1390 (2014)
8. X. Yu, Q. Zhang, Y. Ling, Z. Yang, H. Cheng, Promoted stability and electrocatalytic activity of PtRu electrocatalyst derived from coating by cerium oxide with high oxygen storage capacity. Appl. Surf. Sci. **455**(15), 815–820 (2018)
9. S. Yao, L. Feng, X. Zhao, C. Liu, W. Xing, Pt/C catalysts with narrow size distribution prepared by colloidal-precipitation method for methanol electrooxidation. J. Power Sources **217**(1), 280–286 (2012)
10. D.Z. Mezalira, M. Bron, High stability of low Pt loading high surface area electrocatalysts supported on functionalized carbon nanotubes. J. Power Sources **231**(1), 113–121 (2013)
11. C.Y. He, J.J. Zhang, P.K. Shen, Nitrogen-self-doped graphene-based non-precious metal catalyst with superior performance to Pt/C catalyst toward oxygen reduction reaction. J. Mater. Chem. A **2**(9), 3231–3236 (2014)
12. S. Maass, F. Finsterwalder, G. Frank, R. Hartmann, C. Merten, Carbon support oxidation in PEM fuel cell cathodes. J. Power Sources **176**(2), 444–451 (2008)
13. M.Y. Jing, L.H. Jiang, B.L. Yi, G.Q. Sun, Comparative study of methanol adsorption and electro-oxidation on carbon-supported platinum in acidic and alkaline electrolytes. J. Electroanal. Chem. **688**(1), 172–179 (2013)
14. S. Basri, S.K. Kamarudin, W.R. WanDaud, Z.A. Yaakob, A.H. Hkhadum, Study on kinetic energy of a novel metal composite for anode catalyst in direct methanol fuel cell. Int. J. Energy Res. **39**(2), 181–190 (2015)
15. M. Cai, M.S. Ruthkosky, B. Merzougui, S. Swathirajan, M.P. Balogh, S.H. Oh, Investigation of thermal and electrochemical degradation of fuel cell catalysts. J. Power Sources **160**(2), 977–986 (2006)
16. A.L. Santos, D. Profeti, P. Olivi, Electrooxidation of methanol on Pt microparticles dispersed on SnO_2 thin films. Electrochim. Acta **50**(13), 2615–2621 (2005)
17. S. Chauhan, G. Richards, T. Mori, P. Yan, J.P. Hill, K. Ariga, J. Zou, J. Drennan, Fabrication of nano-structured Pt-loaded cerium oxide nanowire and its anode performance in the methanol electrooxidation reaction. J. Mater. Chem. A **1**(20), 6262–6270 (2013)
18. K. Senevirathne, R. Hui, S. Campbell, S. Ye, J. Zhang, Electrocatalytic activity and durability of Pt/NbO_2 and Pt/Ti_4O_7 nanofibers for PEM fuel cell oxygen reduction reaction. Electrochim. Acta **59**(1), 538–547 (2012)
19. S. Jayaraman, T.F. Jaramillo, S.H. Baeck, E.W. McFarland, Synthesis and characterization of $Pt-WO_3$ films as methanol oxidation catalysts for low-temperature polymer electrolyte membrane fuel cells. J. Phys. Chem. B **109**(48), 22958–22966 (2005)
20. Y.J. Wang, D.P. Wilkinson, J.J. Zhang, Noncarbon support materials for polymer electrolyte membrane fuel cell electrocatalysts. Chem. Rev. **111**(12), 7625–7651 (2011)
21. H.R. Zhao, Y. Wang, Q.H. Tang, L. Wang, H. Zhang, C. Quan, T. Qi, Pt catalyst supported on titanium suboxide for formic acid electrooxidation reaction. Int. J. Hydrog. Energy **39**(18), 9621–9627 (2014)
22. Z. Qiu, H. Huang, J. Du, T. Feng, W.K. Zhang, Y.P. Gan, X.Y. Tao, NbC nanowire-supported Pt nanoparticles as a high performance catalyst for methanol electrooxidation. J. Phys. Chem. C **117**(27), 13770–13775 (2013)
23. Y.L. Zhao, Y.H. Wang, X.Z. Cheng, L. Dong, Y. Zhang, J.B. Zang, Platinum nanoparticles supported on epitaxial TiC/nanodiamond as

an electrocatalyst with enhanced durability for fuel cells. Carbon **67**, 409–416 (2014)

24. K.S. Lee, I.S. Park, Y.H. Cho, D.S. Jung, H.Y. Park, Y.E. Sung, Electrocatalytic activity and stability of Pt supported on Sb doped SnO_2 nanoparticlesfor direct alcohol fuel cells. J. Catal. **258**(1), 143–152 (2008)

25. S. Camillo, J.T.H. Kwan, B. Arman, P.W. David, S. Peter, The stability challenges of oxygen evolving catalysts: towards a common fundamental understanding and mitigation of catalyst degradation. Angew. Chem. Int. Ed. **56**(22), 5994–6021 (2017)

26. G. Simon, K. Olga, M.M. Andrea, J.J.M. Karl, C. Serhiy, Stability limits of tin-based electrocatalyst supports. Sci. Rep. **7**(4595), 1–7 (2017)

27. T. Okanishi, T. Matsui, T. Takeguchi, R. Kikuchi, K. Eguchi, Chemical interaction between Pt and SnO_2 and influence on adsorptive properties of carbon monoxide. Appl. Catal. A **298**(10), 181–187 (2006)

28. T. Binninger, R. Mohamed, A. Patru, K. Waltar, E. Gericke, X. Tuaev, E. Fabbri, P. Levecque, A. Hoell, T.J. Schmidt, Stabilization of Pt nanoparticles due to electrochemical transistor switching of oxide support conductivity. Chem. Mater. **29**(7), 2831–2843 (2017)

29. D.J. Guo, Electrooxidation of ethanol on novel multi-walled carbon nanotube supported platinum–antimony tin oxide nanoparticle catalysts. J. Power Sources **196**(2), 679–682 (2011)

30. S.Q. Song, W.J. Zhou, Z.H. Zhou, L.H. Jiang, G.Q. Sun, Q. Xin, V. Leontidis, S. Kontou, P. Tsiakaras, Direct ethanol PEM fuel cells: the case of platinum based anodes. Int. J. Hydrog. Energy **30**(9), 995–1001 (2005)

31. Y. Lin, S.C. Zhang, S.H. Yan, G.R. Liu, The effect of Sn content in Pt-SnO_2/CNTs for methanol electro-oxidation. Electrochim. Acta **66**(1), 1–6 (2012)

32. A. Bauer, L. Chevallier, R. Hui, S. Cavaliere, J. Zhang, D. Jones, J. Roziere, Synthesis and characterization of Nb-TiO_2 mesoporous microsphere and nanofiber supported Pt catalysts for high temperature PEM fuel cells. Electrochim. Acta **77**(30), 1–7 (2012)

33. W. Li, Z. Pan, Z. Huang, Q. Zhou, Y. Xu, S. Wu, C. Chen, Y. Lin, G. Hu, Pt nanoparticles supported on titanium iron nitride nanotubes prepared as a superior electrocatalysts for methanol electrooxidation. Int. J. Hydrog. Energy **43**(20), 9777–9786 (2018)

34. G.Y. Liu, J.Y. Xu, Y.T. Wang, X.D. Wang, An oxygen evolution catalyst on an antimony doped tin oxide nanowire structured support for proton exchange membrane liquid water electrolysis. J. Mater. Chem. A **3**(41), 20791–20800 (2015)

35. Y.S. Kim, H.S. Jang, W.B. Kim, An efficient composite hybrid catalyst fashioned from Pt nanoparticlesand Sb-doped SnO_2 nanowires for alcohol electro-oxidation. J. Mater. Chem. **20**(30), 7859–7863 (2010)

36. J.Y. Xu, Q.F. Li, M.K. Hansen, E. Christensen, A.L.T. García, G.Y. Liu, X.D. Wang, N.J. Bjerrum, Antimony doped tin oxides and their composites with tin pyrophosphates as catalyst supports for oxygen evolution reaction in proton exchange membrane water electrolysis. Int. J. Hydrog. Energy **37**(24), 18629–18640 (2012)

37. J.Y. Xu, A. David, Q.F. Li, C. Pan, E. Christensen, O.J. Jens, W. Zhang, G.Y. Liu, X.D. Wang, J.B. Niels, Antimony doped tin oxide modified carbon nanotubes as catalyst supports for methanol oxidation and oxygen reduction reactions. J. Mater. Chem. A **1**(34), 9737–9745 (2013)

38. A. Tabet-Aoul, M. Mohamedi, Interrelated functionalities of hierarchically CNT/CeO_2/Pt nanostructured layers: synthesis, characterization, and electroactivity. Phys. Chem. Chem. Phys. **14**(13), 4463–4474 (2012)

39. M. Arentz, V. Stamenkovic, B.B. Blizanac, K.J. Mayrhofer, N.M. Markovic, P.N. Ross, Carbon-supported Pt-Sn electrocatalysts for the anodic oxidation of H_2, CO, and H_2/CO mixtures: Part II: the structure–activity relationship. J. Catal. **232**(2), 402–410 (2005)

40. L.X. Ding, A.L. Wang, G.R. Li, Z.Q. Liu, W.X. Zhao, C.Y. Su, Porous Pt-Ni-P composite nanotube arrays: highly electroactive and durable catalysts for methanol electrooxidation. J. Am. Chem. Soc. **134**(33), 5730–5733 (2012)